

Manipulation of Emission Colors Based on Intrinsic and Extrinsic Magneto-Electroluminescence from Exciplex Organic Light-Emitting Diodes

Zhiyong Pang,^{†,‡} Dali Sun,^{†,‡,‡} Chuang Zhang,^{†,‡} Sangita Baniya,[†] Ohyun Kwon,^{*,§} and Zeev Valy Vardeny^{*,†}

[†]Department of Physics & Astronomy, University of Utah, Salt Lake City, Utah 84112, United States

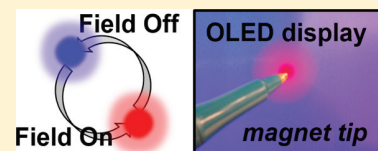
[‡]Department of Physics, North Carolina State University, Raleigh, North Carolina 27695, United States

[§]Samsung Advanced Institute of Technology, Samsung Electronics, Co., Ltd., 130 Samsung-ro, Yeongtong-gu, Suwon-si, Gyeonggi-do 16678, Korea

Supporting Information

ABSTRACT: Exciplex organic light-emitting diodes (XOLEDs) utilize nonemissive triplet excitons via a reverse intersystem crossing process of thermally activated delayed fluorescence. The small energy difference between the lowest singlet and triplet levels of exciplex also allows a magnetic field to manipulate their populations, thereby achieving ultralarge “intrinsic” magneto-electroluminescence (MEL) in XOLEDs. Here we incorporate it into a hybrid type of spintronic device (“hybrid spin-XOLED”), where the XOLED is connected to a magnetic tunnel junction with large magnetoresistance, to introduce an “extrinsic” MEL response that interferes with the “intrinsic” MEL. The ratio between two MEL contributions, the MEL value, and the field response were altered by changing the exciplex layer thickness or actively manipulated by adding another current source that drives the XOLED. Most importantly, by involving two XOLEDs (green and red) in the same circuit, the hybrid spin-XOLED shows a color change when sweeping the magnetic field, which provides an alternative way for future OLED display technologies.

KEYWORDS: organic light-emitting diodes, exciplex, magneto-electroluminescence, organic spintronics, thermally activated delayed fluorescence



Recently, the internal quantum efficiency of organic light-emitting diodes (OLEDs) based on singlet emitters has been substantially boosted by introducing thermally activated delay fluorescence (TADF) compounds, where the energy splitting, ΔE_{ST} , between the lowest singlet (S1) and triplet (T1) exciplex states is sufficiently small to achieve reverse intersystem crossing (RISC) at room temperature.^{1–12} In general, two classes of TADF-based compounds have been developed: the first class shows intramolecular TADF in which RISC occurs intrinsically in a single molecule, whereas the RISC in the second class is intermolecular, where exciplex states are formed by charge transfer (CT) between donor (D) and acceptor (A) molecules in their blend.^{1,2,9,13–19} The intermolecular TADF materials have been extensively used in exciplex OLEDs (XOLEDs), showing very high electroluminescence (EL) quantum yield, color tunability, and enhanced stability, especially when fluorescent emitters are added to the D–A blend.^{1–4,9,11,13,14,20–30} These fluorescent guests lead to a rapid Förster resonance energy transfer from the exciplexes to the designated emitters, which further facilitates RISC from the exciplex triplets and, in turn, enhances the EL performance and device stability.^{25–27,30}

In addition, the intermolecular XOLEDs have shown significant EL intensity enhancement when an external magnetic field is applied.^{31–33} The magneto-EL (MEL) response, which is the relative change of EL intensity upon

the magnetic field, B , has been reported to reach a colossal value of $\sim 4000\%$ in XOLEDs upon “device conditioning”.³³ This is about 3 orders larger than the MEL response in traditional polymer OLEDs based on the spin-mixing between singlet and triplet polaron pairs through hyperfine interaction.³⁴ To explain the extraordinary MEL in the XOLEDs, we showed in previous studies^{31,35} the existence of an additional spin-mixing process, which is due to the difference, $\Delta\nu$, of the spin precession frequencies about the external field between the electron and hole in the exciplex, since they are respectively located on different D and A molecules. This originates from the difference, Δg , of electron and hole g -factors, leading to spin-mixing between singlet and triplet exciplex states via the so-called “ Δg mechanism”.^{36–38} This new spin-mixing mechanism in the exciplex adds to the polaron-pair mechanism of injected carriers and may explain the enhanced MEL response in XOLEDs.³¹

To further explore the potential of exciplex materials for magnetic control of EL emission, we propose here a hybrid spintronics XOLED device (dubbed hybrid spin-XOLED, or spin-XOLED for simplicity), where a spin valve, namely, a magnetic tunnel junction (MTJ), is electrically attached to the

Received: June 2, 2017

Published: July 31, 2017

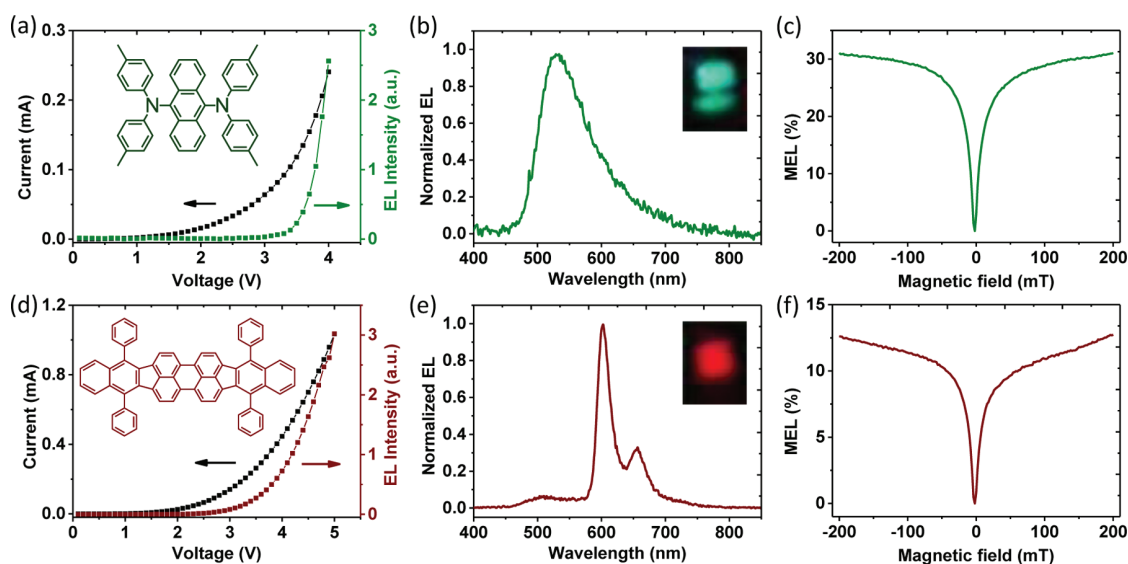


Figure 1. (a) I - V and EL - V characterizations of the XOLED doped with a green emitter, TTPA (inset shows molecular structure). (b) EL spectrum from the green XOLED; inset shows a photo image of the EL emission. (c) Intrinsic $MEL(B)$ response of the XOLED measured at constant bias. (d-f) The same as in (a) to (c) but for the XOLED with a red emitter, DBP (molecular structure and EL photo are shown in insets).

XOLED. This “two-component” binary device has been shown to combine the advantages of both OLED and spin valve devices, which consequently provides similar $MEL(B)$ response as that of a spin-polarized LED.³⁹ Such a device overcomes the limits of conductivity mismatch between ferromagnetic (FM) electrodes and organic semiconductors, which is the main reason for low MEL performance at cryogenic temperatures in conventional spin-OLEDs.⁴⁰ Moreover, in the case of a spin-XOLED the interplay between the large “intrinsic” MEL (i.e., from the XOLED alone) and the additional “extrinsic” MEL (i.e., driven by the MTJ component) responses is very interesting since it brings about a myriad of possibilities for potential magnetic EL manipulation.⁴¹

In this work, we have used N,N,N,N -tetrakis(4-methoxyphenyl)benzidine (MeO-TPD) as the donor and tris[3-(3-pyridyl)mesityl]borane (3TPYMB) as the acceptor in the exciplex blend. The XOLEDs show bright EL emission the color of which could be green or red respectively when introducing 9,10-bis[N,N -di(p -tolyl)amino]anthracene (TTPA) or tetraphenylidibenzoperiflanthene (DBP) as fluorescent emitters. When coupling the XOLED with the MTJ device, two $MEL(B)$ responses (namely, “intrinsic” and “extrinsic” MEL s) are obtained, and the total maximum MEL value (i.e., MEL_{max}) increases by a factor of 2 compared to the “intrinsic” MEL of XOLEDs. Moreover the amplitude and polarity of $MEL(B)$ could be controlled by the interplay between the “intrinsic” and “extrinsic” MEL contributions. This has been achieved, for example, by changing the thickness of the active layer in the XOLED or adding a second driving current through the XOLED component. Importantly, a visible color change has been observed by applying a magnetic field on a spin-XOLED device that contains both green and red XOLEDs.

EXPERIMENTAL SECTION

The XOLEDs were fabricated on patterned indium tin oxide (ITO)-coated glass with a vertically layered structure of ITO/PEDOT:PSS/exciplex/Ca/Al. The ITO substrates were cleaned using ultrasonics with a soap solution, deionized

water, acetone, and methanol in sequence. Subsequently the substrates were treated with oxygen plasma, and then a ~ 30 nm thick hole transport layer PEDOT:PSS (Clevios P VP Al 4083) was deposited by spin-coating at 3000 rpm. Following annealing at 140 °C for 20 min, the films were transferred into a glovebox. All the remaining fabrications were done in the glovebox filled with a nitrogen atmosphere ($H_2O/O_2 < 1$ ppm). The D-A blend active layer was prepared using a solution-based method.³¹ MeO-TPD (99.99%, Lumtec Corporation), 3TPYMB (99.99%, Lumtec Corporation), and the emitter TTPA (99.99%, Lumtec Corporation) or DBP (99.99%, Lumtec Corporation) were dissolved separately in *ortho*-dichlorobenzene (ODCB) solvent at a concentration of 7 mg/mL and stirred overnight. The solutions were then mixed together to prepare the exciplex blend with a weight ratio of 1:4 for the D-A molecules.³¹ The doping of TTPA or DBP emitter was kept at 1 wt %. After that the mixed solution was stirred and spin coated onto the PEDOT:PSS layer at 1000 rpm. Finally the Ca (~ 20 nm) electrode and Al (~ 100 nm)-capped film were thermally evaporated under vacuum (10^{-6} Torr) using a shadow mask. The XOLEDs show a typical brightness of more than 120 cd/m^2 and a current efficiency of >0.5 cd/A (see Figure S1).

The MTJ was fabricated using a shadow mask technique via dc magnetron and ion beam sputtering onto thermally oxidized silicon substrates. The MTJ structure was IrMn/CoFeB/CoFe/MgO/CoFeB/Ta/Pt, where the MgO was used as a tunnel barrier, CoFeB and CoFe were used as FM electrodes, and the antiferromagnetic IrMn was used as the pinning layer. For the fabrication of spin-XOLED, the MTJ was carefully wire-bonded to the XOLED on the same chip. The magnetic field effect measurements were performed at room temperature in a vacuum chamber, which was placed between the two poles of an electromagnet having a field, B , up to 200 mT. The EL spectrum was recorded with a fiber spectrometer (Ocean Optics USB4000). For the magneto-resistance ($MR(B)$) measurement a constant bias was applied to the MTJ, and the current was monitored by a high-current source-measure unit (Keithley 238). The $MR(B)$ is defined as $MR(B) = [R(B)/$

$R(0) - 1]$. For the $MEL(B)$ measurement a constant bias was applied to the XOLED or spin-XOLED, and the EL intensity was monitored with a silicon detector while sweeping B back and forth. An additional constant current source (Keithley 2400) could be applied to the XOLED component when measuring the $MEL(B)$ response from the spin-XOLED. The $MEL(B)$ is defined as $MEL(B) = [EL(B)/EL(0) - 1]$. We note that the PEDOT:PSS layer has a very low resistance and magneto-resistance compared with the XOLED, and its contribution to the $MEL(B)$ is therefore negligible (see Figure S2).

RESULTS AND DISCUSSION

As shown in Figure 1a the green XOLED (TTPA, Figure 1a inset) shows a typical $I-V$ diode response, and the bias onset for EL emission is 3 V. The EL spectrum (Figure 1b) is in the form of a broad band ranging from 500 to 650 nm that originates from the TTPA emission, which is much brighter than the emission from the lowest singlet exciplex state in pristine XOLED.^{25,26} When applying a magnetic field up to 200 mT on the XOLED device, a maximum of $\sim 30\%$ increase in the overall EL intensity was observed, although the bias was kept constant (Figure 1c). We note that this MEL_{\max} value is smaller than that obtained in the pristine XOLED, probably because the EL emission is more efficient here.³⁵ In addition the $MEL(B)$ response has a full width at half-maximum (fwhm) of ~ 25 mT, which agrees well with that of the $MEL(B)$ response in the pristine device. It is interpreted as due to the Δg spin-mixing mechanism in the lowest exciplex singlet-triplet states.^{31,36–38} We note in passing that the value and width of $MEL(B)$ are much larger compared with those in OLEDs based on π -conjugated polymers, where the hyperfine interaction was the dominant spin-mixing mechanism. It is the same reason that the $MEL(B)$ here cannot be from the dopant molecules.³⁵

When changing the emitter from TTPA to DBP (Figure 1d inset), the $I-V$ response of the XOLED does not change much, except that the turn-on voltage is reduced to 2.5 V (Figure 1d). The EL spectrum is now much narrower and red-shifted to ~ 600 nm followed by a vibrational replica at 660 nm (Figure 1e). We conclude that both green and red XOLEDs have been fabricated by doping the appropriate emitters in the MeO-TPD/3TPYMB exciplex host. However, the $MEL(B)$ response in the red XOLED is weaker than that in the green TTPA device, with $MEL_{\max} = 12.5\%$ at $B = 200$ mT (Figure 1f), which may be explained by the different energy transfer efficiencies of these two emitters.^{25,35} In contrast the fwhm of the $MEL(B)$ response in the two XOLEDs remains almost constant (~ 25 mT), indicating the same Δg mechanism for MEL is viable in both devices.³⁸

For achieving an “extrinsic” MEL response we integrated an XOLED together with the MTJ in series to form a spin-XOLED device. Figure 2a shows a typical $MR(B)$ response from the MTJ, and the resistance is lower at large B because the magnetization directions of two FM layers (CoFeB and CoFe) are parallel to each other. The resistance abruptly increases by 50% when the two magnetization directions become antiparallel upon the field sweeping. The “switching field” corresponds to the coercive field of the respective FM electrodes. We therefore expect that in the hybrid spin-XOLED the MR from the MTJ component would change the current through the XOLED component, which would manifest itself by an additional “extrinsic” $MEL(B)$ response. As shown

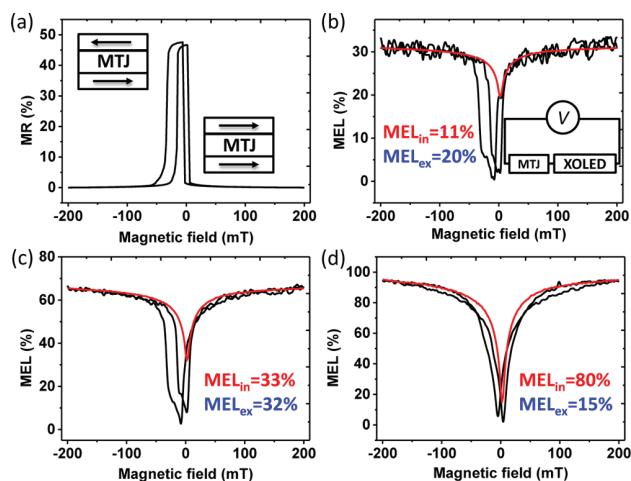


Figure 2. (a) $MR(B)$ response from the MTJ device measured under bias of 0.1 V, showing “hysteretic” behavior. Inset shows the magnetization of FM electrodes. (b, c, d) $MEL(B)$ responses of the spin-XOLEDs at constant applied bias, having various thicknesses of the D–A active layer (~ 50 , ~ 100 , ~ 150 nm, respectively). Inset in (b) shows the equivalent electric circuit. For comparison, red curves correspond to the “intrinsic” $MEL(B)$ from XOLEDs measured without the MTJ component.

in Figure 2b, the spin-XOLED shows a pronounced $MEL(B)$ response up to 30% at $B = 200$ mT, having a field response that is very different from that of the $MEL(B)$ in XOLED alone. In fact the $MEL(B)$ here contains both the hysteretic feature of $MR(B)$ that originates from the MTJ component (“external”, MEL_{ex}) and the intrinsic, nonhysteretic $MEL(B)$ response from the XOLED component (“internal”, MEL_{in} , red curve in Figure 2b).

Since MEL_{ex} and MEL_{in} coexist in these spin-XOLED devices, the $MEL(B)$ response can be manipulated by varying the device preparation and operation conditions. For example, MEL_{ex} is mainly related to the resistance match between the MTJ and XOLED components, as well as to the nonlinearity in the XOLED $I-V$ response,³⁹ whereas MEL_{in} depends on the D–A exciplex materials (and dopant emitter) and the conditioning treatment of the XOLED device.^{32,33} We present below two venues for controlling MEL_{ex} and MEL_{in} in spin-XOLEDs; these include changing the film thickness of the D–A exciplex active layer in the XOLED and using an additional current source to operate this component.

We found that when the active layer thickness was increased from 50 nm to 100 nm, an enhanced $MEL(B)$ of up to 65% was obtained from the corresponding spin-XOLED, as shown in Figure 2c. Both MEL_{ex} ($\sim 33\%$) and MEL_{in} ($\sim 32\%$) are enhanced compared with the device shown in Figure 2b. MEL_{ex} increase is attributed to the increased nonlinearity in the $I-V$ response of the XOLED, whereas the dependence of MEL_{in} on the active layer thickness is consistent with previous studies.^{32,33} The MR would produce more pronounced MEL response when operating in the nonlinear regime of the $I-V$ curve. As shown in Figure 2d, an ultralarge MEL_{max} value up to 95% was achieved in the spin-XOLED device having an active layer thickness of ~ 150 nm. However, MEL_{in} ($\sim 80\%$) becomes dominant in this case, as MEL_{ex} ($\sim 15\%$) is largely diminished by the resistance mismatch between the MTJ ($\sim k\Omega$) and XOLED ($\sim M\Omega$) components. Overall, MEL_{ex} is not related to the EL efficiency of XOLED devices, whereas MEL_{in} increases

with the active layer thickness, possibly due to the low EL efficiency from the thick active layer, which enhances the MEL.

The I - V response of the XOLED shows an ohmic regime with large and constant resistance, which is followed by a space-charge-limited current (SCLC) regime with bipolar injection that generates EL emission. The XOLED resistance R_{LED} drops in the SCLC regime as a power law in V , which produces a nonlinear response in I - V plots, $I \sim V^n$. We can obtain the following equation to explain the MEL_{ex} amplitude, $\text{MEL}_{\text{ex}} \approx \Delta I/I = \Delta R_{\text{MTJ}}/(R_{\text{MTJ}} + R_{\text{LED}}/n)$,³⁹ which shows that the nonlinearity power, n , in the I - V response plays an important role in amplifying the external MEL(B) introduced by the MTJ component. In addition, both R_{LED} and n increase with the thickness of the TADF active layer, and consequently R_{LED}/n may reach a minimum value and, in turn, MEL_{ex} maximizes at an intermediate thickness.

In comparison, MEL_{in} response keeps increasing with the active layer thickness.³³ It is surprising that by adding another resistance, R_{MTJ} , to the same electrical circuit, the MEL_{in} value does not show any obvious decrease compared with that in the XOLED alone. Therefore, the overall MEL response can be optimized at an intermediate thickness, which provides a means to achieve high EL efficiency at the same time. It shows the advantage of hybrid spin-XOLEDs beyond the OLEDs with large MEL but weak EL emission. This strategy also provides another interesting possibility, that is to manipulate the ratio between MEL_{ex} and MEL_{in} , and by that the overall MEL performance may be widely tuned in these hybrid spin-XOLED devices. To this end, the in situ control of MEL and consequently EL emission is more important for display applications (as shown below).

To achieve active control of the MEL(B) response from spin-XOLEDs, a second current source was added to the XOLED component. Under these conditions, the current source drives the XOLED in addition to the previous voltage source that is applied on the entire spin-XOLED device. Moreover the current through the XOLED, I_{LED} , can be adjusted independently to be either in the same or opposite directions to the current through the MTJ in the outside loop, I_{MTJ} (see Figure 3a and b). The MEL(B) response in this case becomes very different depending on the relative values and polarities of I_{LED} and I_{MTJ} . The reason for this “odd” MEL(B) response from the “modified” spin-XOLED device is that both MEL_{ex} (B) amplitude and polarity change between these two current configurations, while MEL_{in} (B) response remains unchanged. MEL_{ex} (B) “sign flip” originates from the MR(B) response of MTJ component, which actually increases or decreases I_{LED} depending on its polarity with respect to that of the XOLED, namely, in the same or opposite directions to it. $\text{MEL}_{\text{ex}} \approx \Delta I/I_{\text{total}} = (\pm)\Delta I_{\text{MTJ}}/((\pm)I_{\text{MTJ}} + I_{\text{LED}})$, considering I_{LED} was usually kept larger than I_{MTJ} in our measurements; the sign change of MEL_{ex} was thereby expected and its amplitude would be smaller than that in Figure 2 (for $I_{\text{LED}} = 0$). Consequently, the current source modulates the EL intensity of the XOLED, whereas the voltage source provides another control element. As shown in Figure 3c, when I_{LED} is gradually increased via the current source, then MEL(B) weakens because MEL_{ex} contribution from I_{MTJ} decreases. However, when I_{LED} is kept constant (Figure 3d), the MEL_{ex} contribution could also be modulated by changing I_{MTJ} , and the overall MEL(B) performance is readily controlled by the applied bias on the spin-XOLED.

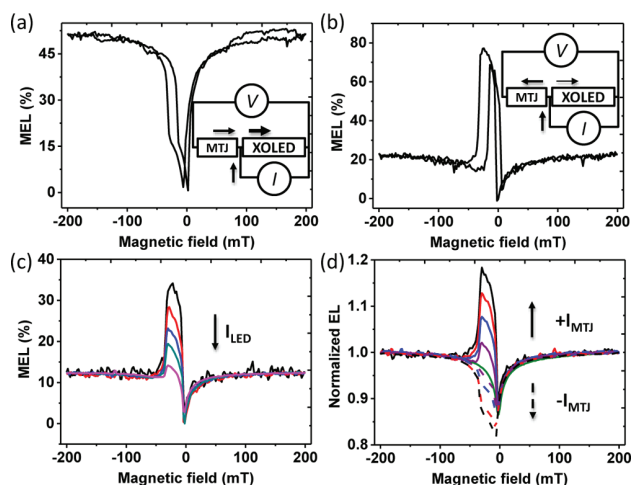


Figure 3. Typical MEL(B) responses in the spin-XOLED with an additional current source that further controls the XOLED component. The additional current I_{LED} is in the same (a) or opposite (b) directions to the current direction in the MTJ, I_{MTJ} . Insets show the respective equivalent electric circuits, where arrows indicate current flows. (c) MEL(B) response in the spin-XOLED with increasing the additional driving current I_{LED} in an “opposite” current configuration. (d) MEL(B) response at various I_{MTJ} (from -0.1 to $+0.1$ mA). The green line indicates the intrinsic MEL from XOLED when the MTJ is disconnected.

Furthermore, we fabricated a “complicated” hybrid spin-XOLED circuit composed of two XOLEDs connected in parallel to the MTJ component, and the two XOLEDs were aligned in “head-to-head” geometry. One of the XOLEDs is based on the TTPA emitter showing green EL, whereas the other XOLED contains DBP, which emits red EL. The overall MEL(B) response in Figure 4a shows relatively small amplitude ($<7.5\%$), with a “bump” near zero field from the MTJ component. As a reference, the device decay after long time operation did not show any obvious change on the EL spectrum except for its intensity. Surprisingly, the EL emission spectrum changes significantly from this spin-XOLED upon the modulation from the magnetic field. Figure 4b displays the EL spectrum at large (small) B field of 160 mT (4 mT), when the magnetization directions of FM electrodes are parallel (antiparallel) in the MTJ. At $B = 160$ mT, the green EL emission (from TTPA) is stronger than the red emission (from DBP), which results in an “olive-like” EL color according to the calculated CIE coordinates (0.41, 0.51). In contrast, the red EL emission becomes more pronounced at $B = 4$ mT, although the total EL intensity is still comparable to that of the large field. The CIE coordinates were calculated to be (0.45, 0.48) in this case, which corresponds to an “orange” EL emission color that differs from the low B field.

Therefore, a visible color change in the EL emission has been achieved by switching the magnetic field on the spin-XOLED, which may be applicable for the future OLED displays industry. In modern displays technologies (Figure 4c left panel), TFTs (thin film transistors) are generally used to control an individual LED unit or individual color filter for a liquid crystal display (LCD) via electric voltage signals. The color control of each pixel is thereby realized by a variety of combinations between the red, green, and blue units. In comparison, the present work shows a visible EL color change (between olive and orange) without using any TFTs, instead achieved by

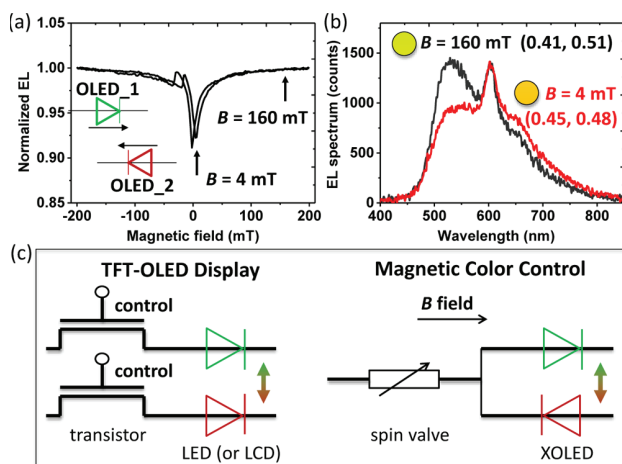


Figure 4. (a) EL(B) intensity from a “complicated” spin-XOLED that contains two XOLEDs connected in parallel to the same MTJ, having currents in the opposite directions. (b) EL spectra measured at $B = 160$ mT (black) and $B = 4$ mT (red) when the MTJ component is at low- and high-resistance states, respectively (see arrows in (a)). The operation conditions were similar to those in Figure 3. Insets show the CIE coordinates and corresponding EL colors. (c) Comparison between two methods of emission color change for displays, namely, the traditional TFT-LED (or LCD) circuit and our method based on the MEL of spin-XOLEDs. The green and red colors represent two-color XOLEDs. The schemes are not supposed to be a practical design of specific devices; they show only the *concept* for magnetically controlled OLED display.

applying an external magnetic field on a spin-XOLED circuit (Figure 4c right panel). This potentially leads to a simple and wireless control of color pixels in the OLED screens.

CONCLUSIONS

In summary, we have reported the design concept and device fabrication of a hybrid spin-XOLED and studied its MEL response under various preparation and operation conditions. This hybrid device is composed of two components, namely, MTJ and XOLED, that are connected in series to obtain the combination of functionalities. The large “intrinsic” MEL_{in} from XOLEDs together with the “extrinsic” MEL_{ex} that originates via the MR(B) of the MTJ provide an opportunity to achieve widely controlled ultralarge MEL response from the spin-XOLEDs. By changing the spin-XOLED geometry and/or operation conditions, nearly 100% total MEL response was obtained, whereby its value and field behavior could be (in situ) controlled. With two or more XOLEDs connected to the same MTJ component, a visible EL color change can be realized; we showed significant EL switching between olive and orange based on two XOLEDs having green TTPA and red DBP emitters, respectively.

Our findings may expand the applications of XOLEDs in the fields of both optoelectronics and spintronics. The advantages of spin-XOLEDs are the large (nearly 100%) and highly controllable MEL, even when the OLEDs are highly efficient. The same concept would allow for magnetic control of basic RGB colors by involving more than a single spin-valve in the electronic system, which is possible but requires specific engineering to achieve better field-dependent color tunability for displays applications. Its limitations when compared with the TFT-OLED technique are obvious, which include the size restriction of device configuration and the cross-talking when

“writing” nearby pixels with a magnetic field. Combining the advanced magnetic storage technique together with OLED display may solve the problems and would be the next step toward industry-level applications, such as applying read/write head coils and voltage pulses.⁴²

ASSOCIATED CONTENT

Supporting Information

The Supporting Information is available free of charge on the ACS Publications website at DOI: 10.1021/acsp Photonics.7b00567.

Typical EL efficiency of XOLED, I - V , and MR of PEDOT:PSS (PDF)

AUTHOR INFORMATION

Corresponding Authors

*E-mail: o.kwon@samsung.com.

*E-mail: val@physics.utah.edu.

ORCID

Zeev Valy Vardeny: 0000-0002-2298-398X

Author Contributions

[†]Z. Pang, D. Sun, and C. Zhang contributed equally to this work.

Notes

The authors declare no competing financial interest.

ACKNOWLEDGMENTS

We acknowledge Drs. W. Han and S. S. Parkin for providing the MTJ devices. This work is supported by the Samsung Global Research Outreach (GRO) program. C.Z. and Z.V. also acknowledge support from the NSF (DMR-1701427). The device fabrication facilities are supported by the NSF-Material Science & Engineering Center (MRSEC) program at the University of Utah (DMR-1121252). Z.P. also thanks the support of the China Scholarship Council (CSC).

REFERENCES

- (1) Uoyama, H.; Goushi, K.; Shizu, K.; Nomura, H.; Adachi, C. Highly efficient organic light-emitting diodes from delayed fluorescence. *Nature* **2012**, *492*, 234–238.
- (2) Goushi, K.; Yoshida, K.; Sato, K.; Adachi, C. Organic light-emitting diodes employing efficient reverse intersystem crossing for triplet-to-singlet state conversion. *Nat. Photonics* **2012**, *6*, 253–258.
- (3) Kaji, H.; Suzuki, H.; Fukushima, T.; Shizu, K.; Suzuki, K.; Kubo, S.; Komino, T.; Oiwa, H.; Suzuki, F.; Wakamiya, A.; Murata, Y.; Adachi, C. Purely organic electroluminescent material realizing 100% conversion from electricity to light. *Nat. Commun.* **2015**, *6*, 8476.
- (4) Hirata, S.; Sakai, Y.; Masui, K.; Tanaka, H.; Lee, S. Y.; Nomura, H.; Nakamura, N.; Yasumatsu, M.; Nakanotani, H.; Zhang, Q.; Shizu, K.; Miyazaki, H.; Adachi, C. Highly efficient blue electroluminescence based on thermally activated delayed fluorescence. *Nat. Mater.* **2015**, *14*, 330–336.
- (5) Zhang, Q.; Li, B.; Huang, S.; Nomura, H.; Tanaka, H.; Adachi, C. Efficient blue organic light-emitting diodes employing thermally activated delayed fluorescence. *Nat. Photonics* **2014**, *8*, 326–332.
- (6) Bergmann, L.; Hedley, G. J.; Baumann, T.; Bräse, S.; Samuel, I. D. W. Direct observation of intersystem crossing in a thermally activated delayed fluorescence copper complex in the solid state. *Sci. Adv.* **2016**, *2*, e1500889.
- (7) Shiu, Y. J.; Cheng, Y. C.; Tsi, W. L.; Wu, C. C.; Chao, C. T.; Lu, C. W.; Chi, Y.; Chen, Y. T.; Liu, S. H.; Chou, P. T. Pyridyl Pyrrolide Boron Complexes: The Facile Generation of Thermally Activated Delayed Fluorescence and Preparation of Organic Light-Emitting Diodes. *Angew. Chem., Int. Ed.* **2016**, *55*, 3017–3021.

- (8) Nakanotani, H.; Furukawa, T.; Morimoto, K.; Adachi, C. Long-range coupling of electron-hole pairs in spatially separated organic donor-acceptor layers. *Sci. Adv.* **2016**, *2*, e1501470.
- (9) Seino, Y.; Inomata, S.; Sasabe, H.; Pu, Y. J.; Kido, J. High-Performance Green OLEDs Using Thermally Activated Delayed Fluorescence with a Power Efficiency of over 100 lm W⁻¹. *Adv. Mater.* **2016**, *28*, 2638–2643.
- (10) Nikolaenko, A. E.; Cass, M.; Bourcet, F.; Mohamad, D.; Roberts, M. Thermally Activated Delayed Fluorescence in Polymers: A New Route toward Highly Efficient Solution Processable OLEDs. *Adv. Mater.* **2015**, *27*, 7236–7240.
- (11) Kim, Y. H.; Wolf, C.; Cho, H.; Jeong, S. H.; Lee, T. W. Highly Efficient, Simplified, Solution-Processed Thermally Activated Delayed-Fluorescence Organic Light-Emitting Diodes. *Adv. Mater.* **2016**, *28*, 734–741.
- (12) Xie, G.; Li, X.; Chen, D.; Wang, Z.; Cai, X.; Chen, D.; Li, Y.; Liu, K.; Cao, Y.; Su, S. J. Evaporation- and Solution-Process-Feasible Highly Efficient Thianthrene-9,9',10,10'-Tetraoxide-Based Thermally Activated Delayed Fluorescence Emitters with Reduced Efficiency Roll-Off. *Adv. Mater.* **2016**, *28*, 181–187.
- (13) Rajamalli, P.; Senthilkumar, N.; Gandeepan, P.; Huang, P.; Huang, M.; Ren-Wu, C.; Yang, C.; Chiu, M.; Chu, L.; Lin, H.; Cheng, C. A New Molecular Design Based on Thermally Activated Delayed Fluorescence for Highly Efficient Organic Light Emitting Diodes. *J. Am. Chem. Soc.* **2016**, *138*, 628–634.
- (14) Hatakeyama, T.; Shiren, K.; Nakajima, K.; Nomura, S.; Nakatsuka, S.; Kinoshita, K.; Ni, J.; Ono, Y.; Ikuta, T. Ultrapure Blue Thermally Activated Delayed Fluorescence Molecules: Efficient HOMO–LUMO Separation by the Multiple Resonance Effect. *Adv. Mater.* **2016**, *28*, 2777–2781.
- (15) Data, P.; Pander, P.; Okazaki, M.; Takeda, Y.; Minakata, S.; Monkman, A. P. Dibenzo[aj]phenazine-Cored Donor–Acceptor–Donor Compounds as Green-to-Red/NIR Thermally Activated Delayed Fluorescence Organic Light Emitters. *Angew. Chem., Int. Ed.* **2016**, *55*, 5739–5744.
- (16) Liu, W.; Chen, J.; Zheng, C.; Wang, K.; Chen, D.; Li, F.; Dong, Y.; Lee, C.; Ou, X.; Zhang, X. Novel Strategy to Develop Exciplex Emitters for High-Performance OLEDs by Employing Thermally Activated Delayed Fluorescence Materials. *Adv. Funct. Mater.* **2016**, *26*, 2002–2008.
- (17) Liu, X. K.; Chen, Z.; Qing, J.; Zhang, W. J.; Wu, B.; Tam, H. L.; Zhu, F.; Zhang, X. H.; Lee, C. S. Remanagement of Singlet and Triplet Excitons in Single-Emissive-Layer Hybrid White Organic Light-Emitting Devices Using Thermally Activated Delayed Fluorescent Blue Exciplex. *Adv. Mater.* **2015**, *27*, 7079–7085.
- (18) Liu, X. K.; Chen, Z.; Zheng, C. J.; Liu, C. L.; Lee, C. S.; Li, F.; Ou, X. M.; Zhang, X. H. Prediction and Design of Efficient Exciplex Emitters for High-Efficiency, Thermally Activated Delayed-Fluorescence Organic Light-Emitting Diodes. *Adv. Mater.* **2015**, *27*, 2378–2383.
- (19) Deotare, P. B.; Chang, W.; Hontz, E.; Congreve, D. N.; Shi, L.; Reuswig, P. D.; Modtland, B.; Bahlke, M. E.; Lee, C. K.; Willard, A. P.; Bulović, V.; Van Voorhis, T.; Baldo, M. A. Nanoscale transport of charge-transfer states in organic donor–acceptor blends. *Nat. Mater.* **2015**, *14*, 1130–1134.
- (20) Li, X. L.; Xie, G.; Liu, M.; Chen, D.; Cai, X.; Peng, J.; Cao, Y.; Su, S. J. High-Efficiency WOLEDs with High Color-Rendering Index based on a Chromaticity-Adjustable Yellow Thermally Activated Delayed Fluorescence Emitter. *Adv. Mater.* **2016**, *28*, 4614–4619.
- (21) Lin, T. A.; Chatterjee, T.; Tsai, W. L.; Lee, W. K.; Wu, M. J.; Jiao, M.; Pan, K. C.; Yi, C. L.; Chung, C. L.; Wong, K. T.; Wu, C. C. Sky-Blue Organic Light Emitting Diode with 37% External Quantum Efficiency Using Thermally Activated Delayed Fluorescence from Spiroacridine-Triazine Hybrid. *Adv. Mater.* **2016**, *28*, 6976–6983.
- (22) Zhang, J.; Ding, D.; Wei, Y.; Han, F.; Xu, H.; Huang, W. Multiphosphine-Oxide Hosts for Ultralow-Voltage-Driven True-Blue Thermally Activated Delayed Fluorescence Diodes with External Quantum Efficiency beyond 20%. *Adv. Mater.* **2016**, *28*, 479–485.
- (23) Li, J.; Ding, D.; Tao, Y.; Wei, Y.; Chen, R.; Xie, L.; Huang, W.; Xu, H. A Significantly Twisted Spirocyclic Phosphine Oxide as a Universal Host for High-Efficiency Full-Color Thermally Activated Delayed Fluorescence Diodes. *Adv. Mater.* **2016**, *28*, 3122–3130.
- (24) Lee, S. Y.; Adachi, C.; Yasuda, T. High-Efficiency Blue Organic Light-Emitting Diodes Based on Thermally Activated Delayed Fluorescence from Phenoxaphosphine and Phenoxathiin Derivatives. *Adv. Mater.* **2016**, *28*, 4626–4631.
- (25) Nakanotani, H.; Higuchi, T.; Furukawa, T.; Masui, K.; Morimoto, K.; Numata, M.; Tanaka, H.; Sagara, Y.; Yasuda, T.; Adachi, C. High-efficiency organic light-emitting diodes with fluorescent emitters. *Nat. Commun.* **2014**, *5*, 4016.
- (26) Furukawa, T.; Nakanotani, H.; Inoue, M.; Adachi, C. Dual enhancement of electroluminescence efficiency and operational stability by rapid upconversion of triplet excitons in OLEDs. *Sci. Rep.* **2015**, *5*, 8429.
- (27) Zhang, D.; Duan, L.; Li, C.; Li, Y.; Li, H.; Zhang, D.; Qiu, Y. High-Efficiency Fluorescent Organic Light-Emitting Devices Using Sensitizing Hosts with a Small Singlet–Triplet Exchange Energy. *Adv. Mater.* **2014**, *26*, 5050–5055.
- (28) Song, W.; Lee, I.; Lee, J. Y. Host Engineering for High Quantum Efficiency Blue and White Fluorescent Organic Light-Emitting Diodes. *Adv. Mater.* **2015**, *27*, 4358–4363.
- (29) Higuchi, T.; Nakanotani, H.; Adachi, C. High-Efficiency White Organic Light-Emitting Diodes Based on a Blue Thermally Activated Delayed Fluorescent Emitter Combined with Green and Red Fluorescent Emitters. *Adv. Mater.* **2015**, *27*, 2019–2023.
- (30) Liu, X. K.; Chen, Z.; Zheng, C. J.; Chen, M.; Liu, W.; Zhang, X. H.; Lee, C. S. Nearly 100% Triplet Harvesting in Conventional Fluorescent Dopant-Based Organic Light-Emitting Devices Through Energy Transfer from Exciplex. *Adv. Mater.* **2015**, *27*, 2025–2030.
- (31) Basel, T.; Sun, D.; Baniya, S.; McLaughlin, R.; Choi, H.; Kwon, O.; Vardeny, Z. V. Magnetic Field Enhancement of Organic Light-Emitting Diodes Based on Electron Donor–Acceptor Exciplex. *Adv. Electron. Mater.* **2016**, *2*, 1500248.
- (32) Lei, Y.; Zhang, Q.; Chen, L.; Ling, Y.; Chen, P.; Song, Q.; Xiong, Z. Ultralarge Magneto-Electroluminescence in Exciplex-Based Devices Driven by Field-Induced Reverse Intersystem Crossing. *Adv. Opt. Mater.* **2016**, *4*, 694–699.
- (33) Wang, Y.; Sahin-Tiras, K.; Harman, N. J.; Wohlgenannt, M.; Flatté, M. E. Immense Magnetic Response of Exciplex Light Emission due to Correlated Spin-Charge Dynamics. *Phys. Rev. X* **2016**, *6*, 011011.
- (34) Macià, F.; Wang, F.; Harmon, N. J.; Kent, A. D.; Wohlgenannt, M.; Flatté, M. E. Organic magneto-electroluminescence for room temperature transduction between magnetic and optical information. *Nat. Commun.* **2014**, *5*, 3609.
- (35) Baniya, S.; Pang, Z.; Sun, D.; Zhai, Y.; Kwon, O.; Choi, H.; Choi, B.; Lee, S.; Vardeny, Z. V. Magnetic Field Effect in Organic Light-Emitting Diodes Based on Electron Donor–Acceptor Exciplex Chromophores Doped with Fluorescent Emitters. *Adv. Funct. Mater.* **2016**, *26*, 6930–6937.
- (36) Wang, F.; Bäessler, H.; Vardeny, Z. V. Magnetic Field Effects in pi-Conjugated Polymer-Fullerene Blends: Evidence for Multiple Components. *Phys. Rev. Lett.* **2008**, *101*, 236805.
- (37) Devir-Wolfman, A. H.; Khachatryan, B.; Gautam, B. R.; Tzabary, L.; Keren, A.; Tessler, N.; Vardeny, Z. V.; Ehrenfreund, E. Short-lived charge-transfer excitons in organic photovoltaic cells studied by high-field magneto-photocurrent. *Nat. Commun.* **2014**, *5*, 4529.
- (38) Zhang, C.; Sun, D.; Sheng, C.-X.; Zhai, Y. X.; Mielczarek, K.; Zakhidov, A.; Vardeny, Z. V. Magnetic field effects in hybrid perovskite devices. *Nat. Phys.* **2015**, *11*, 427–434.
- (39) Sun, D.; Basel, T.; Gautam, B. R.; Han, W.; Jiang, X.; Parkin, S. P.; Vardeny, Z. V. Room-temperature magnetically modulated electroluminescence from hybrid organic/inorganic spintronics devices. *Appl. Phys. Lett.* **2013**, *103*, 042411.
- (40) Nguyen, T. D.; Ehrenfreund, E.; Vardeny, Z. V. Spin-Polarized Light-Emitting Diode Based on an Organic Bipolar Spin Valve. *Science* **2012**, *337*, 204–209.

- (41) Fiederling, R.; Keim, M.; Reuscher, G.; Ossau, W.; Schmidt, G.; Waag, A.; Molenkamp, L. W. Injection and detection of a spin-polarized current in a light-emitting diode. *Nature* **1999**, *402*, 787–790.
- (42) Tokura, Y. Multiferroics as Quantum Electromagnets. *Science* **2006**, *312*, 1481–1482.